Journal of Solid State Chemistry **160,** 353–361 (2001)
doi:10.1006/jssc.2001.9240, available online at http://www.idealibrary.com on IDEAL®

Synthesis, Crystal Structure, and Magnetic Properties of a Novel Layered Manganese Oxide $Sr_2MnGaO_{5+\delta}$

A. M. Abakumov, M. G. Rozova, B. Ph. Pavlyuk, M. V. Lobanov, and E. V. Antipov

Department of Chemistry, Moscow State University, Moscow 119899, Russia
E-mail: abakumov@icr.chem.msu.ru

O. I. Lebedev[1] and G. Van Tendeloo

EMAT, University of Antwerp (RUCA), Groenenborgerlaan 171, B-2020 Antwerp, Belgium

and

O. L. Ignatchik, E. A. Ovtchenkov, Yu. A. Koksharov, and A. N. Vasil'ev

Department of Physics, Moscow State University, Moscow 119899, Russia

Received January 16, 2001; in revised form April 26, 2001; accepted May 11, 2001

New $Sr_2MnGaO_{4.97}$ complex oxide was synthesized by solid state reaction in sealed silica tubes at 950–1000°C. The $Sr_2MnGaO_{4.97}$ crystal structure was refined from X-ray powder diffraction data. $Sr_2MnGaO_{4.97}$ is based on the *Ima*2 brownmillerite-type structure with apically elongated MnO_6 octahedra due to a Jahn–Teller effect. Electron diffraction and high-resolution electron microscopy showed that local ordering of the left- and right-hand chains of GaO_4 tetrahedra in $Sr_2MnGaO_{4.97}$ leads to a superstructure with a doubling of the *b* parameter of the orthorhombic unit cell. The formal oxidation state of Mn (V_{Mn}) can be varied by thermal treatments at elevated oxygen pressure (450°C, 20 bar of O_2). The oxygen insertion induces a structure transformation in oxidized $Sr_2MnGaO_{5.47}$ material with the formation of a tetragonal perovskite-like structure ($a \approx a_p$, $c \approx 2c_p$) with oxygen vacancies located in the Ga layers. The oxidation is accompanied by a significant compression of the Mn–O apical distances and a suppression of the Jahn–Teller deformation. Both $Sr_2MnGaO_{4.97}$ and $Sr_2MnGaO_{5.47}$ can probably be treated as canted antiferromagnets with $T_N \sim 150$ and 80 K, respectively. © 2001 Academic Press

***Key Words*: $Sr_2MnGaO_{5+\delta}$; synthesis; crystal structure; oxygen nonstoichiometry.**

1. INTRODUCTION

Recently we have reported the preparation and the crystal structure of the novel brownmillerites $Ca_2MnGaO_{5+\delta}$ ($\delta = 0.045$–0.09, 0.39) (1). The structure of $Ca_2MnGaO_{5+\delta}$ with $\delta < 0.1$ is built up by layers of MnO_6 octahedra linked by chains of GaO_4 tetrahedra with Ca atoms located at eight-coordinated interstices of this framework. Since the formal Mn valence (V_{Mn}) in these compounds is close to $+3$, the MnO_6 octahedra are subjected to the strong deformation due to a Jahn–Teller effect with four short equatorial Mn–O distances and two long apical ones. The oxidation state of Mn in $Ca_2MnGaO_{5+\delta}$ was varied either by heterovalent replacement of Ga^{3+} for Zn^{2+} or by oxygen insertion after treatment under 80 bar O_2. In the latter case the $Ca_2MnGaO_{5.39}$ compound forms built-up domains of the initial reduced material and the oxidized $Ca_2MnGaO_{5.5}$ ($Ca_4Mn_2Ga_2O_{11}$) phase, which belongs to the brownmillerite $A_nB_{n-1}B'O_{3n-1}$ ($n = 4$) homologous series. The oxygen insertion leads to a decrease of the orthorhombic distortion due to a filling of the vacant anion positions in the (GaO□) layers and the suppression of the Jahn–Teller deformation of the MnO_6 octahedra.

Among brownmillerites of other transition metals there are examples of compounds with Ca or Sr cations in the *A* sublattice demonstrating distinctions in behavior upon the variation of composition or formal valence of the transition metal. For instance, $LaCaCuGaO_5$ retains an orthorhombically distorted structure with $a_0 \approx 4a_P$, $b_0 \approx a_P\sqrt{2}$, $c_0 \approx a_P\sqrt{2}$ upon fluorination while $LaSrCuGaO_5$ undergoes a phase transition into a tetragonal phase with $a_T \approx a_P$, $c_T \approx 2a_P$ due to a random occupation of the anion position in the Ga layers by oxygen, fluorine, and anion vacancies (2). Since both Cu^{2+} and

[1] On leave from Institute of Crystallography, RAS, Leninsky prospekt 59, 117333 Moscow, Russia.

Mn^{3+} cations tend to adopt a Jahn–Teller distorted octahedral environment one may expect similar features to occur in the properties of A_2MnGaO_5 (A = Ca, Sr) compounds. It was a challenge to prepare the $Sr_2MnGaO_{5+\delta}$ brownmillerites and compare their properties with the corresponding Ca-based ones.

2. EXPERIMENTAL

The Sr_2MnGaO_5 compound was prepared by annealing a stoichiometric mixture of SrO, Mn_2O_3, and Ga_2O_3 in alumina crucibles placed into a sealed evacuated silica tube. SrO was obtained by the decomposition of $SrCO_3$ at 900°C in a dynamic vacuum. The initial reagents were intimately mixed in a glove box to prevent the interaction of SrO with CO_2 and H_2O. The samples were annealed at 950°C for 50 h and then at 1000°C for 80 h with intermediate regrinding. After annealing, the samples were quenched in air. Post-annealing treatments were performed in a hermetic stainless steel autoclave at 20–40 bar of oxygen pressure. The cation composition was verified by EDX analysis, performed on different crystallites. The Mn formal valence V_{Mn} and the oxygen content were determined by iodometric titration. The uncertainty in V_{Mn} was evaluated as 2%.

Magnetic susceptibility measurements were performed with a vibrational magnetometer PARC M-155 at $H = 2000$ Oe in the temperature range 4–300 K. Electron paramagnetic resonance (EPR) spectra were collected using an X-band (≈ 9.15 GHz) spectrometer Varian E-4 with a nitrogen variable temperature system E-257 (Varian).

X-ray data for the phase analysis and the refinement of the cell parameters were obtained with a focusing Guinier-camera FR-552 (Cu$K\alpha_1$ radiation, Ge was used as an internal standard). X-ray powder diffraction data for crystal structure determination were collected on a STADI-P diffractometer (Cu$K\alpha_1$ radiation, curved Ge monochromator, transmission mode, linear PSD). The crystal structure computations were carried out using the CSD program package (3). The Rietveld method with pseudo-Voigt profile functions was used for the final refinement. R_P and R_{wP} were calculated after the background was subtracted from the experimental data.

Electron diffraction (ED) and high-resolution electron microscopy (HREM) studies were performed using a JEOL 4000EX instrument. EDX spectra and ED patterns were obtained using a Philips CM20 microscope with a LINK-2000 attachment. Theoretical HREM images were calculated by means of the MacTempas software.

3. RESULTS

3.1. Crystal Structure and Properties

The X-ray diffraction pattern of single-phase Sr_2MnGaO_5 was indexed in a body-centered orthorhombic unit cell with lattice parameters $a = 16.107(2)$ Å, $b = 5.5704(8)$ Å, $c = 5.4181(6)$ Å related to the perovskite subcell by $b \approx 4a_{per}$, $b \approx c \approx a_{per}\sqrt{2}$. Reflections $h0l$: $h, l \neq 2n$ were found to be extinct, in addition to the condition imposed by the lattice centering. The cell parameters and extinctions agree well with a layered brownmillerite-type structure, which is described by the layer sequence

$$-(MnO_2)-(SrO)-(GaO\square)-(SrO)-(MnO_2)-$$

with (most probably) *Ima*2 space symmetry, as it was previously found for other brownmillerites (RACuGaO$_5$ (R=La, Pr, Nd; A=Ca, Sr) (4, 5), Ca_2FeAlO_5 (6), $Sr_2Fe_2O_5$ (7)). The cation ratio Sr:Mn:Ga = 2.08(8):0.96(8):0.96(8) was found to be in good agreement with the bulk composition within standard deviations. The iodometric titration revealed that the formal Mn valence is slightly lower than +3 ($V_{Mn} = +2.94$), thus indicating a small anion deficiency in the compound corresponding to the $Sr_2MnGaO_{4.97}$ formula. This behavior is opposite to that found for $Ca_2MnGaO_{5.045}$ brownmillerite, which exhibits an excess of oxygen when prepared under similar synthesis conditions. Probably, the smaller Ca^{2+} cations ($r = 1.12$ Å, CN = 8) require smaller cavities to be accommodated in the brownmillerite structure and, consequently, shorter Mn–O bonds than the larger Sr^{2+} ones ($r = 1.25$ Å, CN = 8). This shortening is achieved by an increase of oxygen content and V_{Mn} according to the ionic radii of Mn^{2+} (0.82 Å), Mn^{3+} (0.65 Å), and Mn^{4+} (0.54 Å) for CN = 6.

Samples with a higher Mn formal valence were obtained by treatment of the as-prepared $Sr_2MnGaO_{4.97}$ at 20–40 bar oxygen pressure. Annealing of reduced material at 20 bar O_2 and 450°C for 12 h made it possible to obtain a single-phase $Sr_2MnGaO_{5.47}$ compound with $V_{Mn} = +3.94$. The X-ray diffraction pattern of this compound showed that oxygen insertion leads to the formation of a new tetragonal structure with cell parameters $a = 3.8025(8)$ Å, $c = 7.921(2)$ Å. The cell parameters of the tetragonal $Sr_2MnGaO_{5.47}$ phase are connected to the cell parameters of the parent orthorhombic brownmillerite structure as $a_t \approx b_0/\sqrt{2}$, $c_t \approx a_0/2$. The absence of systematic extinctions in the X-ray powder pattern allowed us to propose the most symmetric space group $P4/mmm$.

The crystal structure of $Sr_2MnGaO_{4.97}$ was refined from X-ray powder diffraction data. The refinement was carried out in the *Ima*2 space group and the atomic coordinates for $LaCaCuGaO_5$ were chosen as starting parameters. The refinement yielded a large value of the thermal parameter ($B = 5.6$ Å^2) for the oxygen atom O3 in the (GaO□) layer. The difference Fourier syntheses calculated with the O3 atom removed revealed two approximately equivalent maxima of the electron density with coordinates (3/4, 0.125,

0.387) and (3/4, 0.129, 0.627), positioned at reasonable distances from the Ga atoms. This probably indicates a splitting of the O3 position. According to the electron microscopy results described below, this splitting indeed should take place due to the presence of differently oriented chains of GaO_4 tetrahedra. However, the simultaneous refinement of the coordinates for both oxygen positions assuming the occupancy factors $g = 0.5$ was unsatisfactory and only one of them was left filled with full occupancy for the final refinement. The final refinement was performed with a common thermal parameter for the oxygen atoms. After the refinement an interatomic distance $d(Ga–O3) = 1.72$ Å that is shorter than the usual values for a Ga–O separation (1.82–1.85 Å) was observed. It is important however to note that the refined structure proposes, probably, only a rough description of the real atomic arrangement within the ($GaO\square$) layers, and additional neutron diffraction experiments may reveal fine details of the oxygen distribution within these planes.

The crystal structure of $Sr_2MnGaO_{5.47}$ was calculated assuming *P*4/*mmm* symmetry. The starting model was chosen with a full occupancy of all anion positions according to the "Sr_2MnGaO_6" composition. The refinement of the thermal parameters of oxygen atoms yielded a *B* value of 11.4 Å^2 for the O3 atom in the Ga layer, indicating a partial occupancy of this position. The variation of the occupancy factor and the thermal parameter for this position does not significantly influence the reliability factors, and for the final refinement the occupancy value was fixed to be equal to $g = 0.735$, in accordance with the result of the iodometric titration.

Relatively large thermal parameters were observed for the atoms in the Ga layers for both refined structures. In the $Sr_2MnGaO_{4.97}$ structure it reflects a disorder in the orientation of the Ga–O chains, as was found by electron microscopy. The large thermal parameter of the Ga atoms in $Sr_2MnGaO_{5.47}$ probably indicates static displacements of these cations caused by a variation of their local oxygen environment from tetrahedral to octahedral due to a partial occupancy of the O3 position.

The crystallographic parameters, reliability factors, atomic coordinates, and the most relevant interatomic distances for $Sr_2MnGaO_{4.97}$ and $Sr_2MnGaO_{5.47}$ are listed in the Tables 1, 2, 3, 4, and 5. The experimental, calculated, and difference X-ray patterns are shown in Fig. 1.

The crystal structure of $Sr_2MnGaO_{4.97}$ is represented in Fig. 2a. In this compound the formal Mn oxidation state is close to $+3$ and the coordination environment of the Mn^{3+} cations is subjected to a Jahn–Teller deformation. The MnO_6 octahedron can be described as "apically elongated" with four short equatorial Mn–O distances of 1.91–1.98 Å and two very long apical ones of 2.411 Å. Oxidation to $V_{Mn} = +3.94$ results in the formation of only slightly distorted MnO_6 octahedra as was found in $Sr_2MnGaO_{5.47}$ ($d(Mn–O_{eq}) = 1.90$ Å, $d(Mn–O_{apic}) = 1.95$ Å) (Fig. 2b). The decrease of the Mn–O apical distance results in a compression of the unit cell along the $a_0 = c_t$ axis from 16.12 Å to $7.92 \times 2 = 15.84$ Å in $Sr_2MnGaO_{5.47}$. The increase of the Mn formal valence is also accompanied by a decrease of the average Mn ionic radius, which manifests itself in a contraction of the average $\langle Mn–O \rangle$ separation from 2.10 Å in $Sr_2MnGaO_{4.97}$ to 1.917 Å in $Sr_2MnGaO_{5.47}$.

TABLE 1
Selected Parameters from Rietveld Refinement of X-Ray Powder Data for $Sr_2MnGaO_{4.97}$ and $Sr_2GaO_{5.47}$

	$Sr_2MnGaO_{4.97}$	$Sr_2MnGaO_{5.47}$
Space group	Im*a*2	*P*4/mmm
a, Å	16.1239(3)	3.79962(4)
b, Å	5.5626(1)	
c, Å	5.40262(9)	7.9201(1)
Z	4	1
Cell volume, Å^3	485.08	114.35
Calculated density, g/cm^3	5.202	5.749
2θ range, step, deg.	$8 \le 2\theta \le 108$, 0.01	$9 \le 2\theta \le 109.2$, 0.01
Number of reflections	174	61
Refinable atomic parameters	17	9
R_I, R_P, R_{wP}	0.052, 0.171, 0.119	0.047, 0.142, 0.103

TABLE 2
Positional and Thermal Parameters of Atoms for $Sr_2MnGaO_{4.97}$

Àtom	Position	*x*/*a*	*y*/*b*	*z*/*c*	B_{iso}, Å^2
Sr	8c	0.11084(5)	0.0173(2)	0.505(1)	0.87(2)
Mn	4a	0	0	0	1.15(4)
Ga	4b	$\frac{3}{4}$	0.0701(3)	−0.027(1)	2.63(7)
O1	8c	0.9890(4)	0.258(3)	0.252(4)	1.7(1)
O2	8c	0.1479(3)	0.0617(9)	0.014(3)	1.7(1)
O3	4b	$\frac{3}{4}$	0.161(2)	0.628(2)	1.7(1)

TABLE 3
Selected Interatomic Distances for $Sr_2MnGaO_{4.97}$ (Å)

Sr–O1 2.54(2) × 1	Mn–O1 1.91(2) × 2
Sr–O1 2.61(2) × 1	Mn–O1 1.98(2) × 2
Sr–O1 2.68(1) × 1	Mn–O2 2.411(4) × 2
Sr–O1 2.74(2) × 1	Ga1–O2 1.816(5) × 2
Sr–O2 2.419(5) × 1	Ga1–O3 1.72(1) × 1
Sr–O2 2.73(2) × 1	Ga1–O3 1.93(1) × 1
Sr–O2 2.83(2) × 1	
Sr–O3 2.542(5) × 1	

TABLE 4
Positional and Thermal Parameters of Atoms for $Sr_2MnGaO_{5.47}$

Atom	Position	x/a	y/b	z/c	B_{iso}, Å^2
Sr	2h	$\frac{1}{2}$	$\frac{1}{2}$	0.2624(2)	1.44(3)
Mn	1b	0	0	$\frac{1}{2}$	0.68(9)
Ga	1a	0	0	0	3.7(1)
O1	2e	$\frac{1}{2}$	0	$\frac{1}{2}$	0.7(2)
O2	2g	0	0	0.254(2)	2.7(2)
O3[a]	2f	$\frac{1}{2}$	0	0	4.7(6)

[a] $g = 0.735$ (fixed).

3.2. Magnetic and Resonance Properties

Temperature dependencies of the static magnetic susceptibility of the $Sr_2MnGaO_{4.97}$ and $Sr_2MnGaO_{5.47}$ compounds are shown in Fig. 3.

The curve for the $Sr_2MnGaO_{4.97}$ exhibits a ferromagnetic-like upturn at ~ 150 K with an additional paramagnetic-like contribution visible below ~ 25 K. Our recent neutron powder diffraction data showed that this compound undergoes the transition to AFM state at $T_N \sim 150$K. In this connection the upturn is treated as indication for the canting of the magnetic sublattices induced by Dzyaloshinskii–Moriya interaction, which is allowed by *Ima*2 space symmetry (8). Fit of the data in the paramagnetic region to Curie–Weiss law revealed $\theta \sim -270$ K and effective moment $\mu_{eff} \sim 5.6\mu_B$. The calculated μ_{eff} is slightly higher than the spin-only value $\mu = \sqrt{24} \approx 4.9\mu_B$ expected for the high-spin $3d^4$ $(t_{2g}^3 e_g^1)$ Mn^{+3} ion and close to the value expected for the total spin + orbital moment $\mu = 5.5\mu_B$. However the calculated value may be overestimated since the narrow temperature range of paramagnetic behavior does not make it possible in particular to correctly determine the Van Vleck term.

The magnetic susceptibility of $Sr_2MnGaO_{5.47}$ above $T_c \sim 80$ K also fits the Curie–Weiss law with $\mu_{eff} \sim 4.1\mu_B$ close to the spin-only value $\mu = \sqrt{15} \approx 3.9\mu_B$ for $3d^3$ (t_{2g}^3) Mn^{+4} ion. The sign of $\theta = -255$ K and signal magnitude (on the order of 10^{-2} emu/mole) makes probable the treatment of the compound as canted AFM as well.

Figure 4 shows the room temperature EPR spectrum of the $Sr_2MnGaO_{4.97}$ compound. Two signals may be clearly observed: a broad unstructured asymmetric line (further denoted as I) and a quintet (II) of relatively narrow lines of varying intensity. The broad line has a peak-to-peak linewidth $\Delta H_{pp} = H_R - H_L \approx 2600$Oe and an effective g value of about 1.90. The effective g-factor was determined

TABLE 5
Selected Interatomic Distances for $Sr_2MnGaO_{5.47}$ (Å)

Sr–O1 2.674(1) × 4	Mn–O1 1.900 × 4
Sr–O2 2.6875(3) × 4	Mn–O2 1.95(1) × 2
Sr–O3 2.816(1) × 4	Ga1–O2 2.01(1) × 2
	Ga1–O3 1.900 × 4

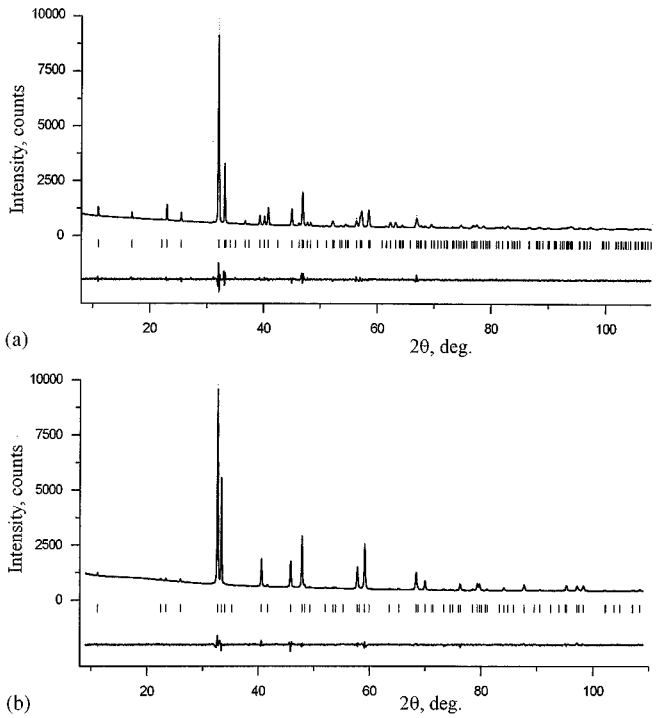

FIG. 1. Experimental, calculated and difference X-ray diffraction profiles for $Sr_2MnGaO_{4.97}$ (a) and $Sr_2MnGaO_{5.47}$ (b).

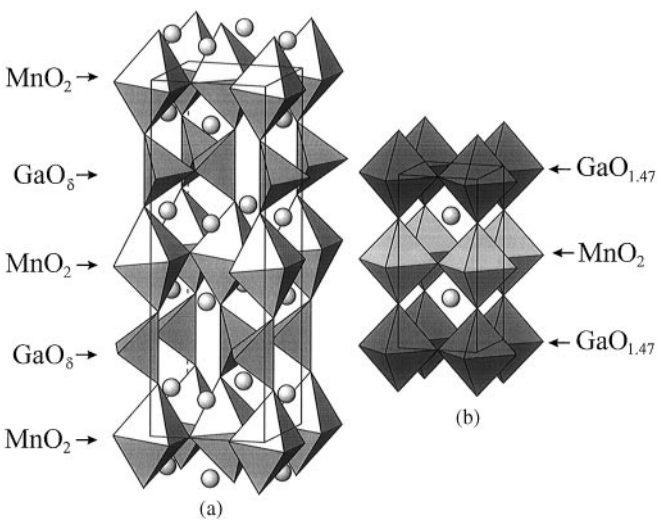

FIG. 2. Crystal structures of $Sr_2MnGaO_{4.97}$ (a) and $Sr_2MnGaO_{5.47}$ (b). Sr atoms are imaged as spheres, oxygen atoms are located at the corners of polyhedra. The occupancy factor for anion positions in the $GaO_{1.47}$ layers is $g = 0.735$.

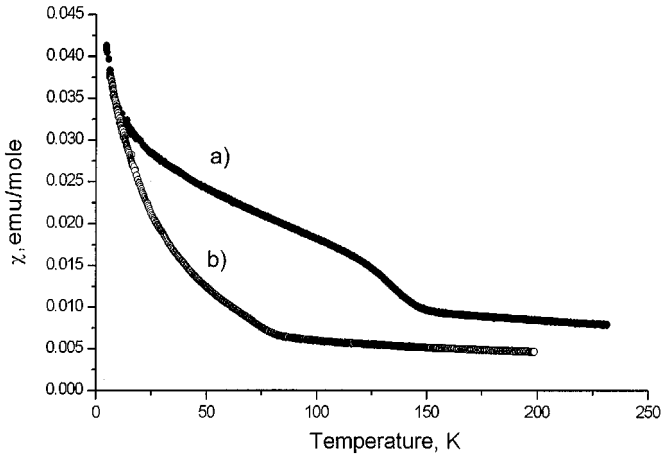

FIG. 3. Temperature dependencies of the static magnetic susceptibility of $Sr_2GaMnO_{4.97}$ (a) and $Sr_2MnGaO_{5.47}$ (b).

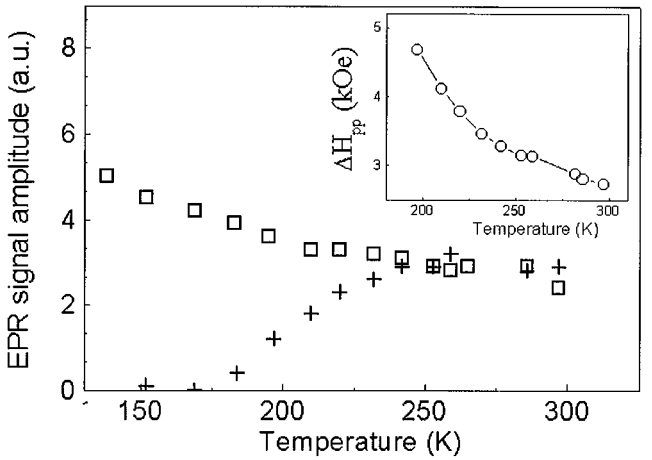

FIG. 5. Thermal variations of the peak-to-peak EPR amplitude for the signal II (squares) and the signal I (crosses). Inset shows the temperature dependence of the peak-to-peak linewidth of line I. The solid line is a guide to the eye.

as $g_{\text{eff}} = 2.0023 \cdot H_e/[(H_R + H_L)/2]$, where H_e is the magnetic field corresponding to a reference free-electron EPR signal $g_e = 2.0023$.

Inset (a) of Fig. 4 shows the detailed structure of the quintet. The spectrum is nearly symmetrical, since intervals between component positions are as follows: $H_A - H_B = 90 \pm 5$ Oe, $H_B - H_C = H_D - H_C = 140 \pm 10$ Oe, $H_E - H_D = 100 \pm 5$ Oe. The noncentral components are relatively narrow: $\Delta H_{AB} = \Delta H_{DE} = 20 \pm 2$ Oe, $\Delta H_{BC} = \Delta H_{CD} = 15 \pm 1$ Oe. The central component is most intense and broadened ($\Delta H_C = 80 \pm 20$ Oe), probably, from the unresolved hyperfine structure. The oxidized sample demonstrates a narrow EPR singlet with $g = 2.00(1)$ and $\Delta H_{pp} = (220 \pm 10)$ Oe (inset (b) of Fig. 4), which is typical of Mn^{4+}.

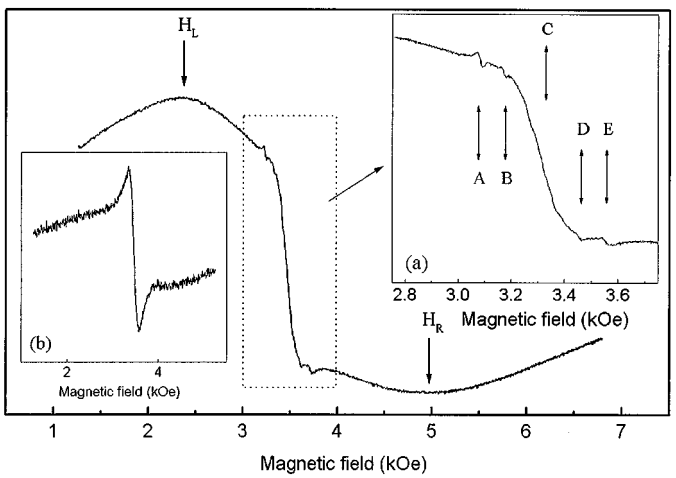

FIG. 4. The room temperature EPR spectrum for $Sr_2GaMnO_{4.97}$. Inset (a) shows the EPR signal for $Sr_2GaMnO_{4.97}$ ascribed to Mn^{2+}. Inset (b) shows the EPR signal for $Sr_2MnGaO_{5.47}$ ascribed to Mn^{4+}.

As the temperature decreases, the line I is broadening and becomes less intense until completely disappears at $T \approx 150$ K. (Fig. 5). The linewidth of line I exceeds 5 kOe below 200 K (inset of Fig. 5), which precludes obtaining meaningful data. In contrast, the linewidth of the II remains nearly temperature independent and the EPR peak-to-peak amplitude slightly increases as temperature decreases (Fig. 5).

Narrow lines in the quintet may be attributed to an EPR fine structure of Mn^{+2} ($S = \frac{5}{2}$) centers in the high-spin (HS) electronic configuration, since a small amount of Mn^{+2} ions is expected from the chemical composition ($V_{Mn} = +2.94$). The EPR spectrum of HS Mn^{2+} in octahedral environment is well known (9). It is characterized by $\Delta m_S = \pm 1$ transitions within the $S = \frac{5}{2}$ multiplet of levels. If the zero-field splitting is much smaller than the Zeeman energy, the spectrum should consist of five lines, which are symmetrical in respect of the central one with $g = 2.00$. In polycrystalline samples the central line, corresponding to transitions within the $m_S = \pm \frac{1}{2}$ doublet, dominates in the spectrum because of the strong angular dependence of other transitions ($\frac{1}{2} \leftrightarrow \frac{3}{2}$, $\frac{3}{2} \leftrightarrow \frac{5}{2}$, $-\frac{1}{2} \leftrightarrow -\frac{3}{2}$, $-\frac{3}{2} \leftrightarrow -\frac{5}{2}$). The extreme noncentral components (A and E lines in the inset of Fig. 4) should be more intense than the residuary two (B and D).

As stated above, the formal Mn valence in the compound studied is close to $+3$. Hence, the EPR signal from Mn^{3+} should be expected. It was suggested that the strong spin–orbit relaxation and the large zero-field splitting preclude a detection of Mn^{3+} ($3d^4$) spectrum by conventional EPR spectrometers (9–11). In manganites with mixed valence of Mn ions a strong EPR signal could be attributed to a complex Mn^{3+}–Mn^{4+} (11, 12). In compounds where the formal valence of Mn is close to $+3$, the EPR signal must be

explained otherwise. A broad EPR line in $LaMnO_3$ (with $\Delta H_{pp} = 2.5$ kOe at room temperature (13)) was ascribed to Mn^{3+} subjected to a tetragonal Jahn–Teller (JT) distortion (14). In that case, the ground state of Mn^{3+} is an orbital singlet with the usual Zeeman effect. The EPR signal of such a JT Mn^{3+} ion is expected to have $g_z \approx 1.95$ and $g_x = g_y \approx 1.99$ (14). For polycrystalline samples with $g_z < g_x = g_y$ and anisotropic linewidth ($\Delta H_z < \Delta H_y \approx \Delta H_z$) the EPR spectrum should resemble line I. Hence, it is reasonable to consider the broad EPR line for $Sr_2GaMnO_{4.97}$ as a signal from JT Mn^{3+} ions. The narrow EPR line for $Sr_2MnGaO_{5.47}$ (inset (b) of Fig. 4) may be ascribed to Mn^{4+} ions. It is known that an EPR signal from Mn^{4+} is relatively narrow and may be easily detected even at room temperature (9, 15). The g-factor for Mn^{4+} (d^3) is isotropic and very close to g_e (9).

The temperature dependence of the EPR line I is typical of antiferromagnets when the Néel temperature approaches from above (16). Its disappearance at 150 K (Fig. 5) agrees with the magnetic susceptibility and neutron diffraction data. The effect of the magnetic transition on line II is not understood clearly. Low-temperature measurements are required.

3.3. Electron Microscopy Investigation

The most relevant electron diffraction patterns of $Sr_2MnGaO_{4.97}$ are shown in Fig. 6. All bright reflections on these patterns can be successfully indexed on the basis of the unit cell determined by X-ray diffraction. The absence of hkl, $h + k + l \neq 2n$ and $h0l$, $h, l \neq 2n$ reflections is compatible with the space group $Ima2$. No extra features such as additional reflections, spot splitting, or extra diffuse intensity were found in the [010]*, [001]*, and [011]* patterns. However, weak spots, which can not be indexed with the brownmillerite unit cell, are present in the [100]* reciprocal space section (Fig. 6a). These spots are positioned at $(0, k/2, l)$ and indicate a doubling of the b parameter. Such a superstructure was previously observed for $YSr_2Cu_2CoO_7$ by electron diffraction and high-resolution electron

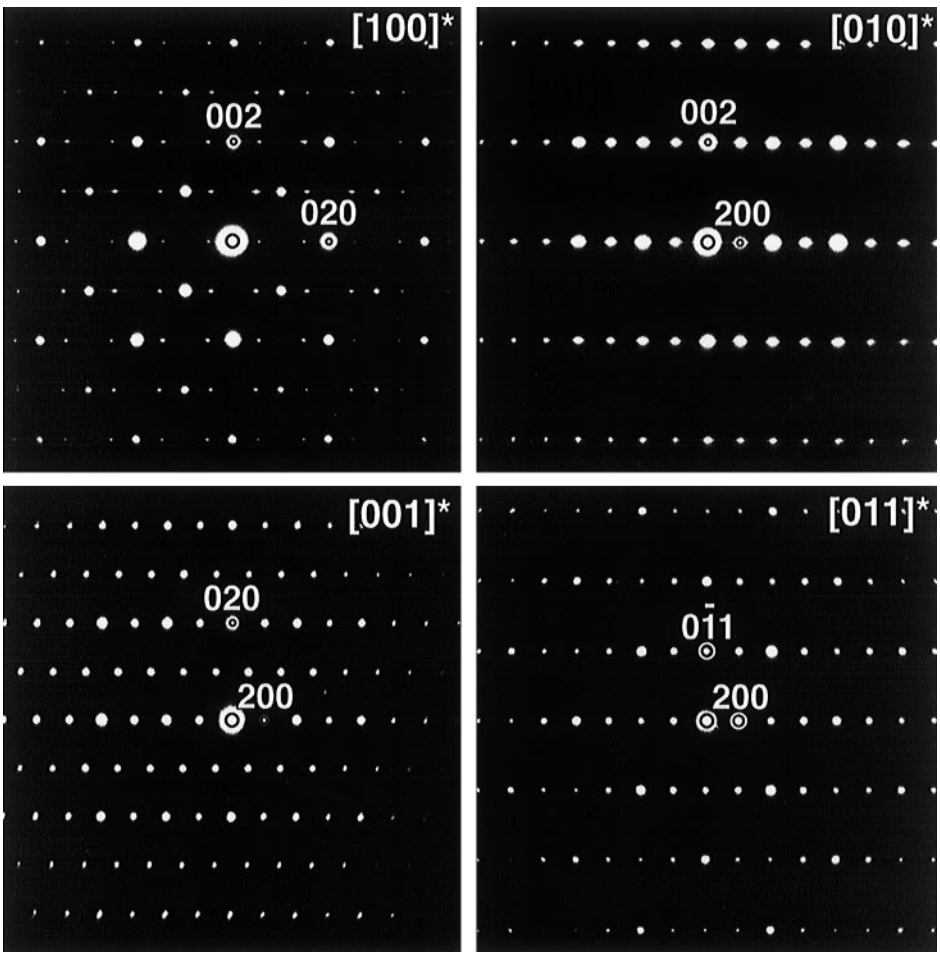

FIG. 6. [100]*, [010]*, [001]*, and [011]* electron diffraction patterns of $Sr_2MnGaO_{4.97}$. Note the presence of weak superlattice reflections in the [100]* ED pattern.

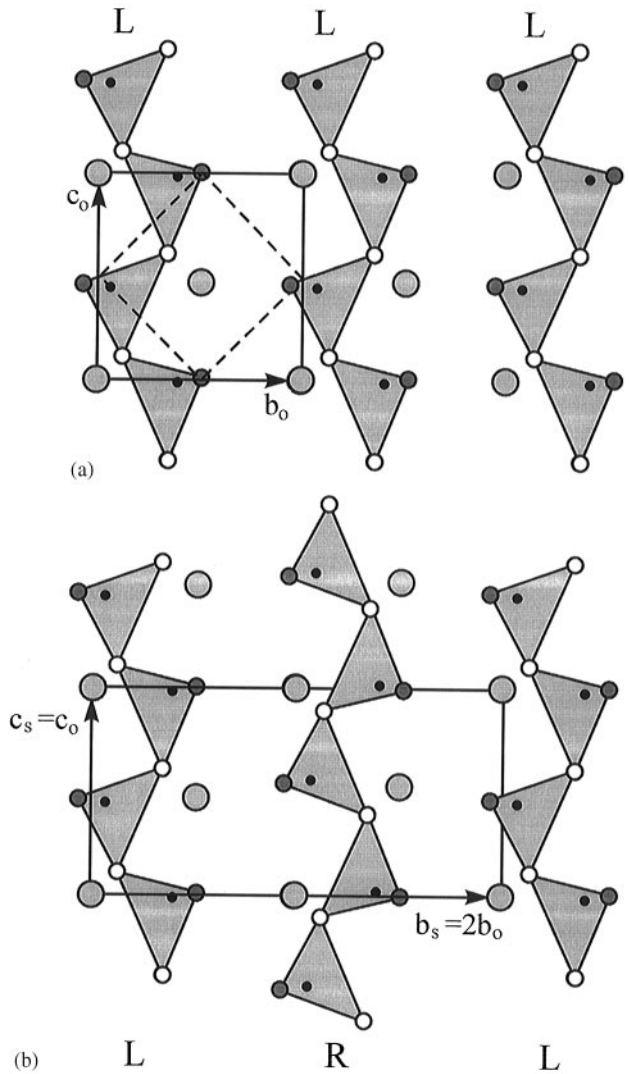

FIG. 7. The models of the structure of (GaO□) layers in (a) the basic brownmillerite structure, all chains being of L type and (b) the superstructure due to ordered alternation of L and R chains along the b_0 axis. Solid lines and circles represent the unit cell and atoms in the initial orthorhombic structure, respectively: large shaded circles correspond to Sr atoms, small black circles to Ga atoms. The shaded triangles represent the projections of GaO_4 tetrahedra. Open circles in the corners of the triangles are oxygen atoms in the (GaO□) plane, shaded circles oxygen atoms above and below the (GaO□) layer. Dashed lines correspond to the tetragonal unit cell of $Sr_2MnGaO_{5.47}$.

microscopy (17). This compound contains Co in a tetrahedral environment and the atomic arrangement of the (CoO□) layers is essentially the same as that of the (GaO□) layer in the brownmillerite. The reciprocal space sections taken along the normal to the (MO□) layer planes for $YSr_2Cu_2CoO_7$ and $Sr_2MnGaO_{4.97}$ show an identical geometry and an intensity distribution that allows us to propose the same model for the appearance of the superstructure in both cases. Two distinct orientations of the chains of the MO_4 tetrahedra are possible. These orientation variants are connected by a mirror plane perpendicular to the direction of the chains, have an identical surrounding, and are therefore energetically equivalent. This was shown also by comparison of the electrostatic energies for brownmillerites containing differently oriented chains (18, 19). Assuming the abbreviations L (left-hand chain) and R (right-hand chain) (17) for the two possibilities of the orientation of the chains, only either L or R chains are present in the *Ima*2 brownmillerite structure. An ordered arrangement of L and R chains necessarily leads to the appearance of a superstructure. If layers of L chains alternate with layers of R chains along the long axis of the brownmillerite unit cell, the I-centered lattice transforms into a primitive one (*Pnma* structure). This is the case for $Ca_2MnGaO_{5+\delta}$ where both *Pnma* and *Ima*2 phases coexist in the same sample as separate crystallites or as microdomains within the same crystallite. In both $YSr_2Cu_2CoO_7$ and $Sr_2MnGaO_{4.97}$ structures L and R chains alternate within the same layer, resulting in a doubling of the *b* parameter, i.e., along the axis normal to the direction of the chain propagation. Figure 7 illustrates the relationship between the parent structure and the superstructure; the corresponding unit cells are outlined. It should be noted that the coordinates of the maxima on the Fourier map of the Ga layer for the $Sr_2MnGaO_{4.97}$ crystal structure correspond to the positions of oxygen atoms in L and R chains, thus confirming the proposed structure model.

The [010] and [011] real space projections of the structure do not make it possible to observe the ordering of L and R chains, and therefore the [010] and [011] HREM images (Fig. 8) can be treated as images of the substructure. L and R chains viewed along these zones produce the same contrast since their projections along the [010] and [011] directions are identical. The [010] image shows a perfect stacking sequence with a repeat period of four layers, compatible with the brownmillerite structure. According to the image simulation, the (MnO_2) layers are reproduced as rows of less bright dots. The [011] image (i.e., along a $[100]_p$ direction of the perovskite subcell) shows a square pattern of dots separated by ≈ 2.8Å. The computer-simulated [010] and [011] images (Fig. 9), calculated using the structure data from Table 2 for different thickness and defocus values, show a remarkable agreement with the experimental images of Fig. 8.

The doubling of the *b* parameter is clearly visible in the HREM image along the [100] zone (Fig. 10). The perovskite subcell is marked by bright dots corresponding to the projections of the columns of Sr or Mn and Ga cations. The superstructure appears as stripes of less bright dots centering the squares of the brightest dots; they are better visible in the thicker part of the crystallite (bottom part of Fig. 10). These stripes propagate along the *c* direction and

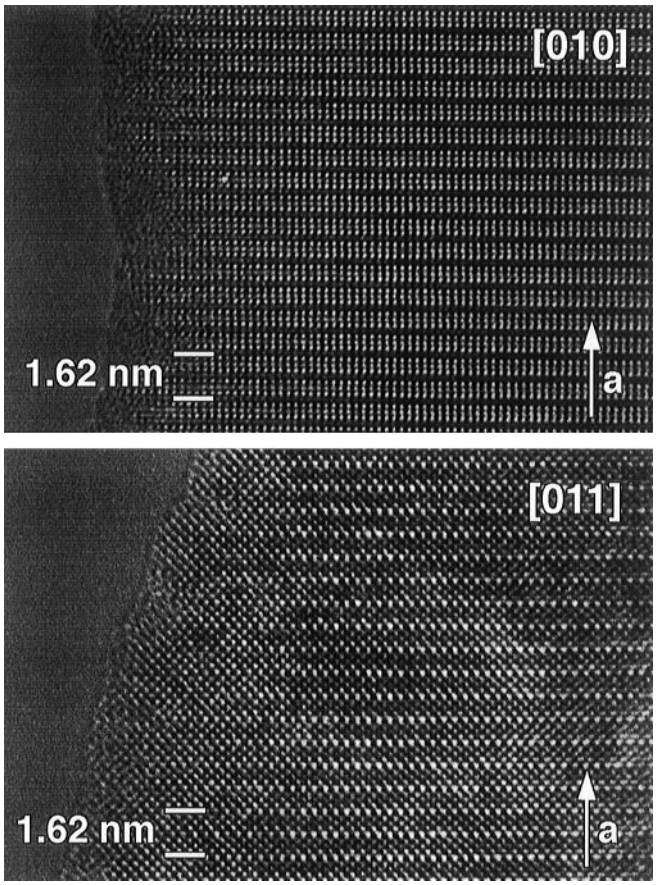

FIG. 8. [010] and [011] HREM images of $Sr_2MnGaO_{4.97}$ showing the perfect brownmillerite structure.

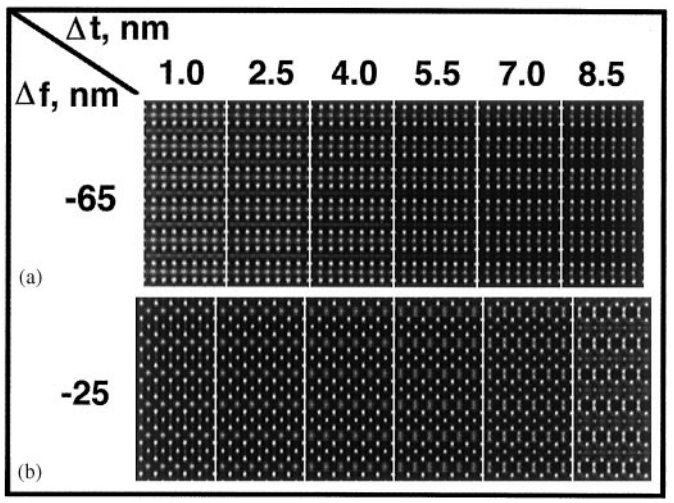

FIG. 9. Matrix of calculated (a) [010] and (b) [011] HREM images using structure data from the X-ray Rietveld refinement of $Sr_2MnGaO_{4.97}$. The images are to be compared with the experimental ones in Fig. 8.

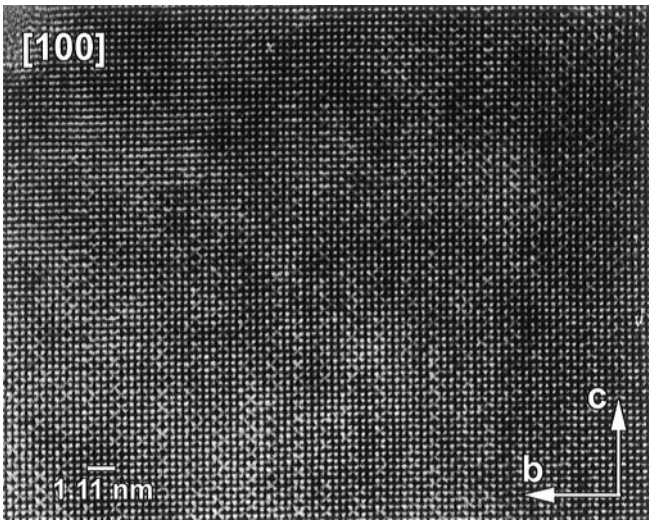

FIG. 10. [100] HREM image of $Sr_2MnGaO_{4.97}$ of the $b_s = 2b_0$ superstructure visible as vertical bright stripes at the bottom part of the image.

are separated by 11.1Å $\approx 2 \times 5.56$Å along the b axis, in agreement with the structure model proposed above. From time to time however the stripes are irregularly spaced; L chains may change into R chains and vice versa. A detailed description of such defects was given by Krekels *et al.* (17) for the $YSr_2Cu_2CoO_7$ compound.

The ill-defined periodicity of the superstructure and the occurrence of planar defects explains the absence of superlattice reflections in the X-ray diffraction patterns, the splitting of the O3 position, and the high values of the thermal parameters of atoms in the Ga layer.

4. DISCUSSION

The similarity between Mn^{3+} and Cu^{2+} cations (similar cation sizes and the ability to adopt strongly Jahn–Teller distorted octahedral surroundings) creates the possibility for the formation of various layered complex oxides with closely related structures. Mn-based analogues were found for the Cu-based Ruddlesden–Popper phases $A_{n+1}Cu_nO_{3n+\delta}((La, Sr)_{n+1}Mn_nO_{3n+1}$ (20)), for the Bi-2201 and Bi-2212 ($Bi_{2-x}Pb_xSr_2MnO_{6+\delta}$ (21, 22), $Bi_{2-x}Pb_xSr_{1.5}Ca_{1.5}Mn_2O_{9-\delta}$(23)), and for La$A$CuGaO$_5$ (A = Ca, Sr) brownmillerites. In the LaACuGaO$_5$ and $A_2MnGaO_{5+\delta}$ brownmillerite structures the MO_6 octahedra are characterized by four short equatorial M–O bonds (1.89–1.96 Å) and two long apical ones (2.24–2.48 Å). Both Mn- and Cu-based compounds can accommodate extra anions at vacant positions in the (GaO□) layers. The insertion of fluorine into LaACuGaO$_5$ occurs as an exchange of O^{2-} for $2F^-$, which does not change the Cu oxidation state in the LaACuGa(O, F)$_{6-\delta}$ oxifluorides.

Because $V_{Cu} = +2$, the CuO_6 octahedra in fluorinated materials retain the distortion that manifests itself in a strong elongation of the perovskite subcell along the apical direction. The intercalation of oxygen in the $A_2MnGaO_{5+\delta}$ compounds is an oxidizing process and leads to an increase of the Mn formal valence up to $+3.78$–3.94. The coordination environment of Mn atoms approaches the perfect octahedron, which is accompanied by a contraction of the perovskite subcell parameter along the direction normal to the (MnO_2) planes.

The transformation of the orthorhombic brownmillerite structure into a tetragonal one with a four times smaller cell volume upon insertion of additional anions was previously observed for fluorinated $LaSrCuGaO_5$ (2). The orthorhombic distortion in the brownmillerite takes place due to the ordering of oxygen atoms and anion vacancies in the Ga layers. The fluorination is accompanied by a random occupation of anion positions in the Ga layers by oxygen, fluorine, and anion vacancies, leading to a suppression of the orthorhombicity. Obviously, the same reason leads to the structure transformation in the strongly oxidized $Sr_2MnGaO_{5.47}$. However, for both $LaCaCuGaO_5$ and Ca_2MnGaO_5 the insertion of extra F or O, respectively, does not make it possible to achieve the transformation into a tetragonal structure and the compounds remain orthorhombic but with a reduced degree of distortion.

ACKNOWLEDGMENTS

The authors are grateful to D. V. Sheptyakov, A. M. Balagurov, and C. Geibel for helpful discussions. The work was done with the help of the RFBR program (Projects 00-03-32392a and 99-02-17823), the SNSF Foundation (Grant 7SUPJ062190.00), CRDF (Project 2256), INTAS (Project 99-0155), NWO (Project 047-008-012), and the Program IUAP 4/10 of the Belgium government. M. V. L. is grateful to the ICDD (2000 Crystallography Scholarship Award). A.M.A. is grateful to the scientific council of Moscow State University for the research fellowship.

REFERENCES

1. A. M. Abakumov, M. G. Rozova, B.Ph. Pavlyuk, M. V. Lobanov, E. V. Antipov, O. I. Lebedev, G. Van Tendeloo, D. V. Sheptyakov, A. M. Balagurov, and F. Bourée, *J. Solid State Chem.* **158,** 100 (2001).
2. J. Hadermann, G. Van Tendeloo, A. M. Abakumov, B.Ph. Pavlyuk, M. Rozova, and E. V. Antipov, *Int. J. Inorg. Mater.* **2,** 493 (2001).
3. L. G. Akselrud, Yu. N. Grin, P. Yu. Zavalij, V. K. Pecharsky, and V. S. Fundamentsky, Thes. report on 12th ECM, Moscow, p. 155 (1989).
4. J. T. Vaughey, J. B. Wiley, and K. R. Poppelmeier, *Z. Anorg. Allgem. Chem.* **598/599,** 321 (1991).
5. G. Roth, P. Adelmann, R. Knitter, S. Massing, and Th. Wolf, *J. Solid State Chem.* **99,** 376 (1992).
6. A. A. Colville and S. Geller, *Acta Crystallogr. Sect. B* **27,** 2311 (1971).
7. M. Harder and Hk. Müller-Buschbaum, *Z. Anorg. Allgem. Chem.* **464,** 169 (1980)
8. E. A. Turov, "Physical Properties of Magnetically Ordered Crystals," Moscow (1963). [In Russian]
9. A. Abragam and B. Bleaney, "Electron Paramagnetic Resonance of Transition Ions." Oxford Univ. Press, New York (1970).
10. C. B. Azzoni, M. Catti, A. Paleari, and C. Pogliani, *J. Phys.: Condens. Matter* **9,** 3931 (1997).
11. A. Shengelaya, G.-M. Zhao, H. Keller, and K. A. Müller, *Phys. Rev. Lett.* **77,** 5296 (1996).
12. S. B. Oseroff, M. Torikachvili, J. Singley, S. Ali, S.-W. Cheong, and S. Schultz, *Phys. Rev. B* **53,** 6521 (1996).
13. E. Granado, N. O. Moreno, A. Garcia, J. A. Sanjurjo, C. Rettori, I. Torriani, S. B. Oseroff, J. J. Neumeier, K. J. McClellan, S.-W. Cheong, and Y. Tokura, *Phys. Rev. B* **58,** 11,435 (1998).
14. V. A. Ivanshin, J. Deisenhofer, H.-A. Krug von Nidda, A. Loidl, A. A. Mukhin, A. M. Balbashov, and M. E. Eremin, *Phys. Rev. B* **61,** 6213 (2000).
15. M. T. Causa, G. Alejandro, M. Tovar, P. G. Pagliuso, C. Rettori, S. B. Oseroff, and M. A. Subramanian, *J. Appl. Phys.* **85,** 5408 (1999).
16. M. S. Seehra and D. L. Huber, *in* "Magnetism and Magnetic Materials —1974" (C. D. Graham, Jr., G. H. Landler, and J. J. Rhyne, Eds.), AIP Conf. Proc. No. 24. Am. Inst. of Phys. New York (1975), and references therein.
17. T. Krekels, O. Milat, G. Van Tendeloo, S. Amelinckx, T. G. N. Babu, A. J. Wright, and C. Greaves, *J. Solid State Chem.* **105,** 313 (1993).
18. R. Hoppe, *Angew. Chem.* **78,** 52 (1966).
19. R. Hoppe, *Adv. Fluorine Chem.* **6,** 387 (1972).
20. R. Mahesh, R. Mahendiran, A. K. Raychaudhury, and C. N. R. Rao, *J. Solid State Chem.* **122,** 448 (1996).
21. J. M. Tarascon, Y. LePage, and W. R. McKinnon, *Eur. J. Solid State Chem.* **27,** 81 (1990).
22. J. M. Tarascon, Y. LePage, W. R. McKinnon, R. Ramesh, M. Eibschutz, E. Tselepis, E. Wang, and G. W. Hull, *Physica C* **167,** 20 (1990).
23. M. Hervieu, C. Michel, D. Pelloquin, A. Maignan, and B. Raveau, *J. Solid State Chem.* **132,** 420 (1997).